BIOCHEMISTRY
including biophysical chemistry & molecular biology

Article

pubs.acs.org/biochemistry

Crystal and Solution Structure Analysis of FhuD2 from *Staphylococcus aureus* in Multiple Unliganded Conformations and Bound to Ferrioxamine-B

Krzysztof J. Podkowa,[†] Lee-Ann K. Briere,[†] David E. Heinrichs,[‡] and Brian H. Shilton*[,†]

[†]Department of Biochemistry and [‡]Department of Microbiology and Immunology, The University of Western Ontario, London, Ontario, Canada N6A 5C1

Supporting Information

ABSTRACT: Iron acquisition is a central process for virtually all organisms. In *Staphylococcus aureus*, FhuD2 is a lipoprotein that is a high-affinity receptor for iron-bound hydroxamate siderophores. In this study, FhuD2 was crystallized bound to ferrioxamine-B (FXB), and also in its ligand-free state; the latter structures are the first for hydroxamate-binding receptors within this protein family. The structure of the FhuD2−FXB conformation shows that residues W197 and R199 from the C-terminal domain donate hydrogen bonds to the hydroxamate oxygens, and a ring of aromatic residues cradles the aliphatic arms connecting the hydroxamate moieties of the siderophore. The available ligand-bound structures of FhuD from *Escherichia coli* and YfiY from *Bacillus cereus* show that, despite a high degree of structural conservation, three protein families have evolved with critical siderophore binding residues on either the C-terminal domain (*S. aureus*), the N-terminal domain (*E. coli*), or both (*B. cereus*). Unliganded FhuD2 was crystallized in five conformations related by rigid body movements of the N- and C-terminal domains. Small-angle X-ray scattering (SAXS) indicates that the solution conformation of unliganded FhuD2 is more compact than the conformations observed in crystals. The ligand-induced conformational changes for FhuD2 in solution are relatively modest and depend on the identity of the siderophore. The crystallographic and SAXS results are used to discuss roles for the liganded and unliganded forms of FhuD2 in the siderophore transport mechanism.

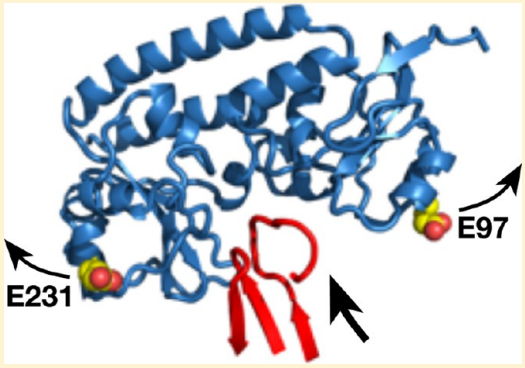

Microorganisms require iron to survive. Although iron is an abundant element, free ferric iron is present only at very low concentrations because of the formation of insoluble iron hydroxides in an oxidizing environment at neutral pH. In host tissues, iron is actively sequestered by cells, further decreasing the amount of available iron. Thus, microorganisms require high-affinity active uptake systems to acquire iron in a host environment. Siderophores are low-molecular weight chelating compounds that bind ferric iron with exceptionally high affinity and are one way that microorganisms scavenge iron from their environment. The ferric hydroxamate uptake (Fhu) system of *Staphylococcus aureus* catalyzes the uptake of hydroxamate-type siderophores; it is comprised of an integral membrane complex, $FhuBGC_2$, which is a member of the ATP binding cassette (ABC) superfamily, and the primary receptors for hydroxamate siderophores, FhuD1 and FhuD2. FhuD1 and FhuD2 are membrane-bound lipoproteins that bind hydroxamate-type iron siderophores with micromolar to nanomolar affinity.[1,2] Once the sample is bound to FhuD1 or FhuD2, a productive interaction with $FhuBGC_2$ leads to movement of the siderophore across the membrane, where the iron is released and used by the cell.

S. aureus is unable to synthesize its own hydroxamate siderophores, and therefore, the Fhu system has evolved to allow *S. aureus* to use siderophores created by other microorganisms in the environment. The Fhu system is upregulated under iron-limited conditions, and FhuD2 was shown to be important for high levels of bacterial proliferation *in vivo*.[3] The role of the *S. aureus* Fhu system in bacterial pathogenesis has led to the identification of FhuD2 as a vaccine candidate. Indeed, mice pretreated with FhuD2 protein produced anti-FhuD2 antibodies that mediated opsonophagocytosis of *S. aureus* and that, when passively transferred, could effectively reduce the bacterial burden in a kidney abscess model of *S. aureus* challenge.[3] The Fhu system can transport a variety of structurally diverse siderophores and is of interest because it is responsible for the uptake of iron-linked siderophore antibiotics ("sideromycins") such as albomycin and salmycin.[4] A detailed understanding of the enzymatic steps involved in Fhu-mediated iron uptake will permit strategies aimed at interfering with the system, or using it to mediate uptake of "Trojan Horse" molecules.

A central question in the ABC transporter field is the mechanism by which ATP hydrolysis is coupled to ligand

Received: October 1, 2013
Revised: March 7, 2014
Published: March 8, 2014

   dx.doi.org/10.1021/bi401349d | *Biochemistry* 2014, 53, 2017−2031

translocation. For ABC-type importers such as the Fhu system, binding of ligand to the peripheral binding protein provokes ATP hydrolysis by the integral membrane complex and leads to release of the ligand from the binding protein and movement through the transporter into the cytosol; however, the individual steps in the process are not understood. In terms of its architecture, $FhuBGC_2$ represents a typical ABC-type solute import system, with two integral transmembrane domains (FhuBG) and two attached ATP binding cassettes ($FhuC_2$). However, a significant difference between the Fhu system and many ABC-type importers is that the binding proteins, FhuD1 and FhuD2, appear to undergo only a relatively small conformational change when they bind ligand, as assessed by solution small-angle X-ray scattering (SAXS).[1,2] Most ABC-type import systems include a class I or class II solute binding protein (SBP) that is characterized by a two-domain structure, with the domains connected by a flexible hinge and the ligand binding site located above the hinge and between the domains.[5] For these proteins, ligand binding leads to a large conformational change that is required for full stimulation of the membrane-bound ATPase.[6,7] FhuD1 and FhuD2 are "class III" binding proteins[8,9] in which the two domains are connected by an α-helical segment. The biological significance of this difference in class III SBP structure is not obvious, and the relatively small conformational change observed upon ligand binding by FhuD1 and FhuD2 has implications for the transport mechanism; in particular, with a relatively small conformational change, it is not clear how binding of a ligand to FhuD1 or FhuD2 regulates ATP hydrolysis by the membrane complex, $FhuBGC_2$.

To gain insight into the ligand-induced structural changes in *S. aureus* FhuD2, we have determined the structure of FhuD2 both alone and in complex with the iron hydroxamate siderophore, ferrioxamine-B (FXB). The structure of FXB-bound FhuD2 shows how the protein recognizes the common hydroxamate features of the ligand and is therefore able to accommodate a variety of hydroxamate siderophores in its binding site. Despite the overall structural homology with *Escherichia coli* FhuD,[10] the critical hydroxamate-binding residues are present in the C-terminal domain of FhuD2, whereas they are part of the N-terminal domain in *E. coli* FhuD. For unliganded FhuD2, we have crystallized both the native protein and a reductively methylated version, which provided crystals that diffracted to beyond 2.5 Å resolution. The native and methylated versions of FhuD2 provided five distinct conformations of unliganded FhuD2. The distinct conformations in the crystal lattice are consistent with relatively minor energetic differences, and the observed extended conformation undoubtedly plays a critical role in the transport mechanism. The solution conformations of FhuD2 bound to four siderophores (aerobactin, coprogen, FXB, and ferrichrome) are each slightly different, with the aerobactin complex closely resembling what is observed for unliganded FhuD2 in solution. These results are used to discuss the role of the unliganded and ligand-bound forms of FhuD2 in the transport mechanism.

EXPERIMENTAL PROCEDURES

Expression and Purification of FhuD2Δ24 and FhuD2Δ43. FhuD2Δ24, which constitutes the FhuD2 protein with the signal sequence and lipid attachment site removed (i.e., the first 24 residues), was expressed as a glutathione *S*-transferase fusion in an *E. coli* BL21(DE3) background. GST-FhuD2Δ24 fusions were isolated using glutathione affinity chromatography, and the glutathione *S*-transferase (GST) moiety was removed by cleavage with tobacco etch virus (TEV) protease and purified as previously described.[1] FhuD2Δ43 has 20 additional residues removed from the N-terminus; the protein was expressed and purified by the same procedure that was used for FhuD2Δ24.

For the incorporation of selenomethionine, a single colony of freshly transformed BL21(DE3) harboring plasmid pMTS37_DH1 was used to inoculate 100 mL of LB broth containing 100 μg/mL ampicillin and grown overnight at 37 °C; 1 mL of the overnight culture was then used to inoculate 1 L of prewarmed (37 °C) M9 medium supplemented with 2 mM $MgSO_4$, 20 μM $CaCl_2$, 15.1 μM $Fe_2(SO_4)_3$, 380 μM thiamine-HCl, and 0.4% (w/v) glucose. When the OD_{600} reached 0.5, the following amino acids were added to the medium: lysine-HCl, phenylalanine, and threonine (each at 0.1 g/L) and leucine, isoleucine, valine, and selenomethionine (each at 0.05 g/L). The cells were grown to an OD_{600} of 0.6, induced with IPTG (100 μg/mL), and harvested after 6 h at 37 °C. For the purification of Se-Met-substituted FhuD2Δ43, all buffers were supplemented with 20 mM DTT.

Reductive Methylation of Lysine Residues. The procedure followed for reductive methylation was similar to that described by Rayment.[11] FhuD2Δ43 was dialyzed overnight against 200 mM sodium phosphate (pH 7.5). A 1 M solution of formaldehyde was prepared from 37 to 40% formaldehyde (BDH, analytical reagent grade) containing 10% methanol as a stabilizer. Note that the use of methanol-free formaldehyde is recommended in the original method;[11] however, we found that the low concentrations of methanol had no undesirable effects on the reaction. Borane dimethylamine complex [BDMA (Sigma-Aldrich)] was used as the reducing agent. Formaldehyde and BDMA solutions were both prepared fresh.

The protein sample, at a concentration of 8 mg/mL, was placed in a 14 mL culture tube wrapped in aluminum foil and kept at 4 °C for the duration of the reaction. For every 1 mL of protein, 50 μL of 1 M BDMA and 100 μL of a 1 M formaldehyde solution (a 10-fold molar excess over the number of amino groups) were added while the mixture was being stirred. The reaction was allowed to proceed for 2 h, and then addition of formaldehyde and BDMA was repeated. After 2 h, an additional 25 μL of the 1 M BDMA solution was added, and the solution was dialyzed against deionized water overnight. The protein solution was subsequently concentrated to 20 mg/mL using 5K molecular weight cutoff centrifugal ultrafiltration devices (Amicon Ultra, Millipore), flash-frozen in liquid N_2, and stored at −80 °C. The degree of substitution was assessed by mass spectrometry of the reductively methylated and unmodified FhuD2 and Se-Met FhuD2: the differences were 1234.4 for FhuD2 and 1233.8 for Se-Met FhuD2, which corresponds to 88 methyl groups. There were 46 amines on the protein (45 lysyl ε-amino groups and the N-terminal α-amino group), yielding 96% modification.

Fluorescence titrations were used to measure the ligand binding affinities of methylated FhuD2Δ43 and compare them to the affinities of the unmethylated versions. The titrations were conducted in 10 mM sodium phosphate and 150 mM KCl (pH 7.5) at 24 °C. Data were analyzed as described by Sebulsky et al.[1]

Crystallization. For our initial crystallization trials, we used the FhuDΔ24 construct, in which the 24 N-terminal residues of the protein were deleted; these residues comprised the signal

anchor sequence as well as the lipid attachment site. FhuDΔ24 was extremely soluble and crystallized from 3.5 to 3.8 M ammonium sulfate (pH 3.5) in the presence and absence of ferrichrome. Crystals of unliganded FhuD2Δ24 diffracted to 3.5 Å from beamline X8C at the National Synchrotron Light Source, but diffraction from crystals of ferrichrome-bound FhuD2Δ24 was barely detectable: the diffraction pattern at very low resolution indicated that the unit cell was exceptionally large. In an effort to improve the crystals of both liganded and unliganded FhuD2, another construct was created, FhuD2Δ43, in which 19 additional residues were deleted from the N-terminus. According to our previous sequence alignment of FhuD2 with *E. coli* FhuD,[1] these N-terminal residues are not present in *E. coli* FhuD, and they are not part of the functional protein core of *S. aureus* FhuD2. The FhuD2Δ43 protein is stable and binds ferrioxamine-B (FXB, or iron-loaded Desferal) and ferrichrome with the same affinity as the FhuD2Δ24 construct (Table 1). FhuD2Δ43 crystallized under conditions similar to those under which FhuD2Δ24 crystallized. The deletion of these N-terminal residues resulted in a significant improvement in the diffraction of ligand-bound FhuD2, with crystals of the ferrichrome−FhuD2Δ43 complex diffracting past 6.5 Å resolution using a laboratory source; however, crystals of unliganded FhuD2 were not improved by the deletion of the N-terminal residues.

Table 1. Siderophore Binding Affinities of FhuD2 Constructs

protein	K_D of ferrichrome (μM)	K_D of ferrioxamine-B (μM)
FhuD2Δ24[a]	0.02	0.05
FhuD2Δ43[b]	0.026 ± 0.002	0.034 ± 0.009
methylated FhuD2Δ43[b]	0.027 ± 0.005	0.075 ± 0.012

[a]Values from ref 1. [b]Average of three determinations ± the standard deviation.

Reductive methylation of FhuD2Δ43 was used to generate new crystals. Methylated FhuD2Δ43 would not crystallize from ammonium sulfate, but new crystallization conditions were found using the "precipitant synergy" screen.[12] Methylated FhuD2Δ43 crystals were grown from solutions of 20% (w/v) PEG 3350, 25% (w/v) PEG 400, 100 mM $MgCl_2$, and 100 mM Tris-HCl (pH 8.5), with a protein concentration of 10 mg/mL at 18 °C.

To obtain FXB-bound FhuD2Δ43, "surface entropy reduction"[13] was used, with three entropy-reducing mutations introduced into the protein: K117A, K118A, and K121A. The protein (26 mg/mL) was crystallized by vapor diffusion with a 1.1:1 Fe-FXB:FhuD2Δ43(K177A/K118A/K121A) ratio against a reservoir of 2.6 M NaCl, 100 mM imidazole, and 250 mM $Zn(OAc)_2$ (pH 8.0).

Structure Solution and Refinement. Crystallographic data were collected at beamline X8C of the Brookhaven National Laboratory. Crystals of reductively methylated and Se-Met-labeled FhuD2 were used initially to determine the structure. These crystals contained two molecules in the asymmetric unit. Selenium positions were located and refined, and initial phases were calculated using BnP.[14] The selenium positions were used to calculate the transformation required for 2-fold NCS averaging, after which the electron density maps could be interpreted and partial models of the two molecules were built using Arp/wArp.[15] Pieces from the two molecules were combined to produce a complete single molecule, which was refined with CNS,[16] initially with strict noncrystallographic symmetry (NCS) constraints. When the complete model was partially refined, NCS constraints were relaxed, and the refinement continued with restraints. At that point, it was evident that the domains in the two NCS-related molecules were in slightly different positions relative to each other, but it was not exactly clear whether there was a single hinge region or multiple hinge regions. For NCS-restrained refinement, the protein was divided into four different domains comprising residues 53−136, 137−183, 184−285, and 286−302. Three

Table 2. Data Collection and Refinement Statistics for FhuD2

	unliganded FhuD2Δ24	FXB-Bound FhuD2Δ43
space group	*I*422	$P2_1$
unit cell	$a = b = 207.5070$ Å, $c = 162.8170$ Å	$a = 81.3426$ Å, $b = 78.9963$ Å, $c = 116.8108$ Å, $\beta = 109.8717°$
wavelength (Å)	1.1000	1.1000
resolution[a] (Å)	24.7−3.5 (3.63−3.50)	45−2.4 (2.53−2.40)
no. of observations[a]	285366	161695 (16405)
no. of unique observations[a]	22693	50153 (6402)
completeness[a]	100.0 (100.0)	91.9 (81.2)
mean $I/\sigma I$[a]	14.7	16.1 (2.7)
R_{merge}[a]	0.047 (0.222)	0.062 (0.278)
final model	A and B, residues 25−302; C, residues 29−302; 65 SO_4^{2-}	A−D, residues 47−302; 4 FXB; 56 Zn^{2+}; 478 solvent
R/R_{free}	0.2201/0.2807	0.198/0.229
root-mean-square deviation		
bond lengths (Å)	0.011	0.002
bond angles (deg)	1.568	0.673
B factor[b] (Å^2)		
all atoms	143.7	37.5
main chain	141.7	36.6
side chain	145.7	38.3
ligand	176.5 (sulfate)	38.2 (FXB), 61.6 (Zn^{2+})
water	–	33.0

[a]Values in parentheses are for the highest-resolution shell. [b]Restrained isotropic *B* factor refinement.

dx.doi.org/10.1021/bi401349d | *Biochemistry* 2014, 53, 2017−2031

rounds of NCS-restrained refinement brought R and R_{free} to 0.216 and 0.303, respectively; the final five rounds of refinement were conducted without NCS restraints and yielded R and R_{free} values of 0.216 and 0.264, respectively.

The second crystal form of unliganded FhuD2 was produced from unmethylated FhuD2Δ24. The crystals diffracted to 3.5 Å (Table 2), and the structure was determined by molecular replacement using the structure of methylated and unliganded FhuD2 as a search model. The three molecules in the asymmetric unit associated through their C-terminal domains, with the "unstructured" region of the N-terminus (residues 24−46) mediating contacts between crystallographically related trimers. After rigid body refinement, R and R_{free} were both approximately 0.45. At this point, NCS restraints had not been applied, but it was clear that they would be required for further refinement given the modest resolution of the data.

To avoid biasing the final structure by applying inappropriate domain boundaries for NCS restraints, refinement proceeded as follows. To establish if and where domain movements had occurred, the three molecules were each divided into nine sections of 30 residues each, and the structure was subjected to rigid body refinement using these 27 rigid groups with no NCS restraints; this refinement decreased R to 0.34 and R_{free} to 0.38, a marked improvement. The resulting structures were then analyzed for domain motions using the DynDom server.[17] When each of the B and C chains were compared with the A chain, the program found essentially two rigid groups, the first comprising residues 49−163 and 272−294 and the second group consisting of residues 164−271 and 295−300. Refinement of the structure proceeded with NCS restraints applied with 13 restraint groups, again to avoid biasing the refinement toward a strictly rigid domain movement.

The crystals of FhuD2Δ43 bound to FXB were twinned (pseudomerohedral). The data could be processed, but not successfully merged, using space group $C222_1$ with the following cell dimensions: a = 81.2278 Å, b = 219.4483 Å, and c = 79.0067 Å. Alternatively, the data could be processed and merged using space group $P2_1$ with the following unit cell dimensions: a = 81.3426 Å, b = 78.9963 Å, c = 116.8108 Å, and β = 109.87° (Table 2). The structure of methylated FhuD2 was used as a model to find a molecular replacement solution with Phaser.[18] The structure was refined using Phenix[19] with the twin law $(-h, -k, h + l)$; the estimated fraction of the twin was 0.35. The crystals of FXB-bound FhuD2 contained four identical molecules in the asymmetric unit, with root-mean-square (rms) distances between CA positions of approximately 0.03 Å. The initial electron density maps for the protein components were unambiguous, but electron density for bound FXB was initially rather poor. During refinement, large peaks in difference Fourier maps indicated the position of the four iron atoms, which were incorporated into the structures. The basic features of the FXB were then visible and made more interpretable by averaging among the four NCS-related molecules (Figure 2A). FXB has three hydroxamate moieties that can coordinate the iron to produce 16 geometric isomers.[20] The following process was used to build a single isomer into the averaged $2F_o - F_c$ electron density maps. First, the electron density indicated a right-handed propeller configuration around the iron atom, reducing the number of possible isomers to eight. Second, the central hydroxamate (number 2) could be positioned on the basis of two tubes of electron density connecting it to the "terminal" hydroxamates (numbers 1 and 3). Third, the aminopentane group attached to hydroxamate number 1 must point upward, out of the binding site, and it appeared that there was weak electron density for the aminopentane moiety adjacent to the side chain of Y210. Therefore, FXB was built into the structure as this single isomer (Figure 2B), although the quality of the electron density for the bound FXB, even after full refinement, was such that other isomers are likely bound as relatively minor species. Given the modest resolution of the structure, and the relatively poor electron density for FXB, restraints were incorporated into the refinement that maintained the characteristic octahedral geometry for the liganding hydroxamates observed in high-resolution small molecule structures.[21]

Crystal structures were deposited in the Protein Data Bank (PDB) as entries 4FKM for unliganded and reductively methylated FhuD2Δ43; 4FNA for native, unmodified FhuD2Δ24; and 4FIL for FhuD2Δ43(K177A/K118A/K121A) bound to ferrioxamine-B.

SAXS Data Collection and Analysis. SAXS data were collected at the Advanced Photon Source, beamline ID-18 (BioCAT). The sample temperature was 20 °C, and the protein solution was moved continuously through a 1 mm quartz capillary during measurement to minimize the effects of radiation damage. The FhuD2 concentration was 5.4 mg/mL. Data were collected at 1455 mm using a CCD detector with X-rays at a wavelength of 1.03 Å, to cover the momentum transfer range (Q) from 0.08 to 3.5 nm^{-1}, where Q is defined as $4\pi \sin \theta/\lambda$ (2θ is the scattering angle and λ the wavelength of the radiation). For each sample, five 10 s exposures that consisted of three measurements from the protein solution bracketed by two measurements of the buffer solution were recorded. Data were integrated using Fit2D (http://www.esrf.fr/computing/scientific/FIT2D) and further processed in Excel: the three protein solution curves and two background buffer curves were inspected and averaged, and the background buffer curve was subtracted from the protein solution curve to yield scattering from the hydrated protein.

Values for the forward (zero angle) scattering, $I(0)$, and the radius of gyration, R_g, were determined from the SAXS curves using the indirect transform method in GNOM,[22] with the same Q range for all data sets ($0.034\ Å^{-1} < Q < 0.35\ Å^{-1}$). For each sample, the Porod volume was calculated with Primus[23] using data up to the asymptotic region in a Porod plot [$Q^4 \times I(Q)$ vs Q], which corresponded to a maximal Q value of 0.131 $Å^{-1}$ in all cases.[24] The V_c parameter was determined using R_g and $I(0)$ values to fill in missing low-angle data, and then integrating a $Q \times I(Q)$ versus Q curve to obtain the total scattered intensity.[25] The FoXS server was used to match crystal structures to solution scattering data.[26]

Sequence Analysis. *S. aureus* FhuD2 and *E. coli* FhuD sequences were used to search the nonredundant protein database, and the two groups of related sequences were imported into Jalview.[27] The entire collection was realigned using TCoffee,[28] and highly similar sequences were removed. At this point, it became clear that the arginine positions in *S. aureus* FhuD2 and *E. coli* FhuD were not conserved in all of the sequences. One such sequence, *Bacillus cereus* YfiY, indicated a PDB structure as its source (PDB entry 3TNY), and the corresponding structure showed two arginine residues, at novel positions, binding the siderophore hydroxamates. The sequences were then reordered on the basis of the position of the liganding arginine residues. Phylogenetic analysis was conducted using the same sequence alignment with the

Phylogeny.fr server,[29] and the output was put into graphical format using FigTree.

RESULTS

FhuD2 is able to bind a number of different hydroxamate siderophores and has been crystallized and determined bound to ferrichrome.[9] To date, however, a major limitation of our understanding of how these proteins function to promote ATP hydrolysis that is dependent upon ligand binding is the lack of an unliganded structure for the hydroxamate-binding proteins in this superfamily. This is especially important because our previous SAXS experiments with FhuD2 indicated a relatively small change in the solution conformation of FhuD2 upon binding hydroxamate siderophores, and the solution structure of FhuD2 appeared to be slightly different for each of four siderophores tested.[1] To investigate ligand-dependent conformational changes in further detail, we determined the structure of FhuD2 bound to desferrioxamine-B (FXB) and compared this to two different crystal structures that we determined for unliganded FhuD2 that contained the protein in five different conformations. The unliganded structures are the first reported for the hydroxamate-binding FhuD homologues and are used to identify changes in FhuD2 conformation that are anticipated to be critical for regulating ATP hydrolysis in the Fhu transporter.

Binding of Desferrioxamine-B (FXB) by FhuD2. FhuD2 is a lipoprotein, tethered to the membrane by a diacylglycerol modification at C18, and because the extreme N-terminal region is most likely unstructured, constructs with N-terminal deletions, either 24 (FhuD2Δ24) or 43 residues (FhuD2Δ43), were used for crystallization. Both constructs had the same ligand binding affinities (Table 1). Diffracting crystals of FXB-bound FhuD2Δ43 were produced by surface entropy reduction:[13] three surface lysyl residues, K117, K118, and K121, were mutated to alanine to produce crystals of the FhuD2−FXB complex that diffracted to 2.4 Å (Table 2).

The hydroxamates of FXB represent the common feature of the FXB isomers as well as the other siderophores bound by FhuD2. The three FXB hydroxamates are bound to FhuD2 by residues R199 and W197 (Figures 1 and 2). The side chain of R199 plays the key role in hydroxamate binding. Hydrogens from NH1 and NH2 of R199 bind to oxygens of hydroxamate numbers 1 and 2, while a second hydrogen from NH2 binds to the amide oxygen (O23) of the siderophore (Figure 2). The second hydrogen of NH1 donates a hydrogen bond to the main chain carbonyl oxygen of W197, while NE of R199 donates a hydrogen bond to the side chain oxygen of D184. Thus, all five polar hydrogens of the R199 side chain are used to anchor the siderophore to the surface of FhuD2 through a hydrogen bond network. In addition, NE1 of W197 donates a hydrogen bond to the oxygen of hydroxamate number 3. W197 was recognized as a conserved residue in sequences of FhuD1, FhuD2, and related proteins from Gram-positive bacteria, and mutation to alanine severely weakened the ability of *S. aureus* to grow using either aerobactin, coprogen, FXB, ferrichrome, or rhodotorulic acid.[1]

The aliphatic portions of the siderophore interact with a ring of aromatic residues that line the binding site, including Y110, Y130, F186, Y191, Y193, W197, W225, W279, and Y280 (Figure 2C). The highly specific hydrogen bonding interactions with the hydroxamates, combined with the ring of aromatic residues that facilitate relatively nonspecific interactions, allows FhuD2 to bind to other hydroxamate siderophores. In this

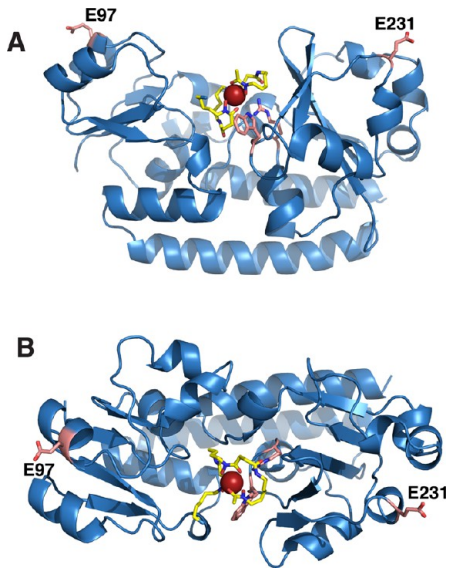

Figure 1. FhuD2 in complex with ferrioxamine-B (FXB). Two views of FhuD2 bound to FXB, related by a 90° rotation about the horizontal axis. The FXB siderophore is shown with yellow carbon atoms; the side chain carbons of two key hydroxamate-interacting residues, W197 and R199, are colored pink. The side chains of E97 and E231, two conserved residues that are critical for siderophore transport,[1] are also colored pink.

regard, the current structure of the FhuD2−FXB complex can be compared with that of FhuD2 bound to ferrichrome[9] (Figure 3). As with FXB, both W197 and R199 make hydrogen bonds to hydroxamate oxygens of ferrichrome. In contrast, siderophore moieties other than the iron and hydroxamates are accommodated differently in the two complexes. The peptide functions of ferrichrome are located outside of the binding site and make relatively few contacts with FhuD2, whereas the arms of FXB are located deeper in the binding site and make numerous contacts with the protein; on this basis, there are several changes in binding site residues in the two complexes (Figure 3). First, the loop harboring F186, which contacts both ferrichrome and FXB, moves approximately 3 Å to accommodate the bulkier FXB; in conjunction with the change in the structure of the loop (residues 185−189), the conformation of the Y191 side chain changes. The other significant adjustment occurs in the side chain of W279, which adopts completely different rotomer conformations in the two structures.

Alternative Binding Site Configurations in FhuD2-Related Proteins. FhuD2 is related to *E. coli* FhuD: the three-dimensional architecture and secondary structure are conserved between *S. aureus* FhuD2 and *E. coli* FhuD, as is the basic chemistry of siderophore binding, but a striking difference between the two proteins is that the siderophore binding functionality is found primarily on the N-terminal domain in *E. coli* FhuD but on the C-terminal domain of *S. aureus* FhuD2. Thus, R199 and W197 on the C-terminal domain of *S. aureus* FhuD2 are replaced with R84 and Y106, respectively, on the N-terminal domain of *E. coli* FhuD. Similarly, residues that interact with the aliphatic portions of the siderophore are found on the C-terminal domain of FhuD2, while they are present on the N-terminal domain of FhuD.

To look for conserved features in the FhuD family of proteins, the sequences of *E. coli* FhuD and *S. aureus* FhuD2 were used to search the nonredundant protein sequence

dx.doi.org/10.1021/bi401349d | *Biochemistry* 2014, 53, 2017−2031

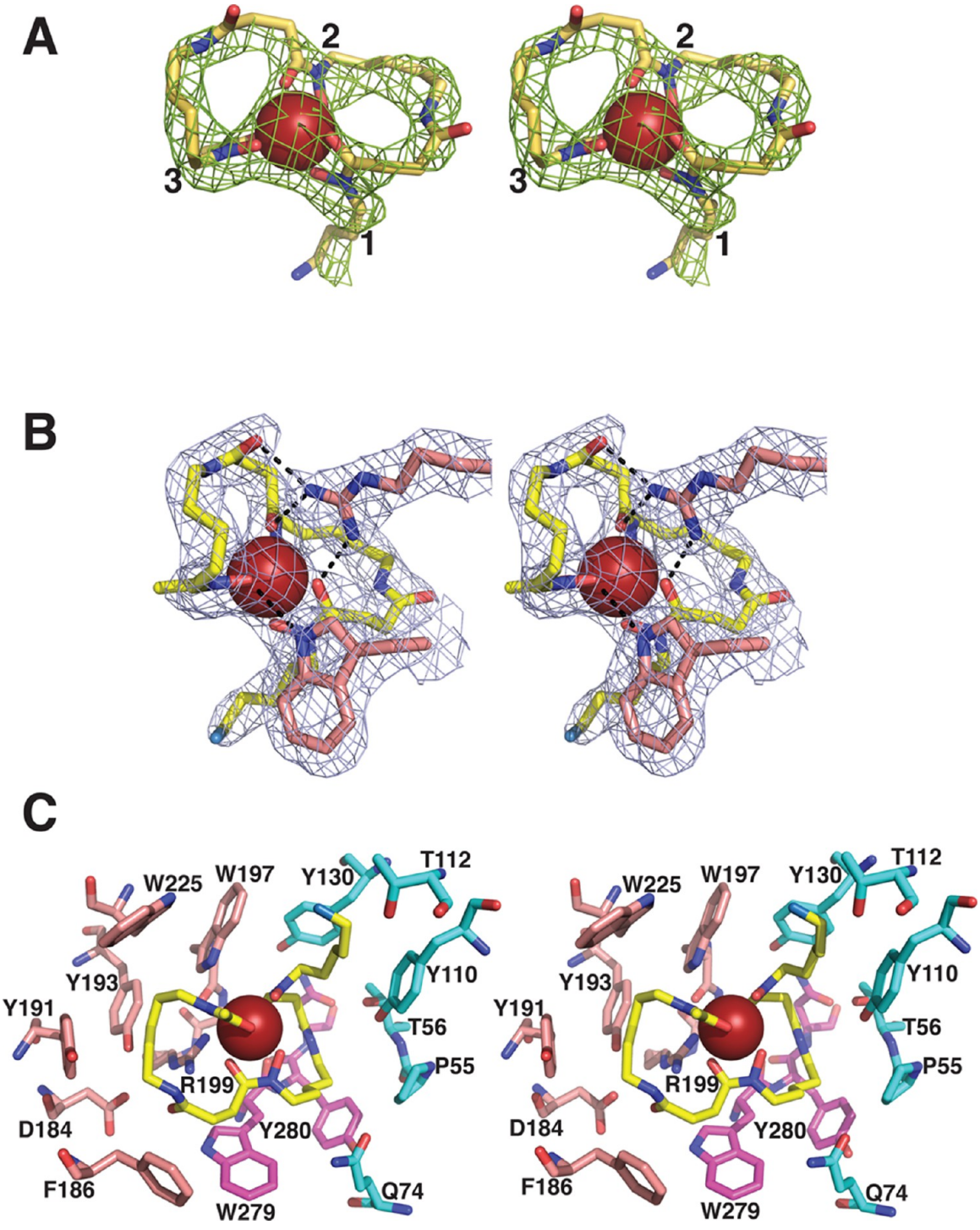

Figure 2. Structure of ferrioxamine-B and interactions with FhuD2. (A) Ferrioxamine-B (FXB) with the initial $2F_o - F_c$ electron density map (contoured at 1σ) obtained by averaging the electron density in the four NCS-related molecules. At that stage, the structure had been partially refined (R = 27.2, and R_{free} = 29.6) and the iron atoms added. (B) Different view of FXB showing the final refined $2F_o - F_c$ electron density. Hydrogen bonding between the hydroxamate oxygens and side chains of W197 and R199 is shown as black dashed lines. (C) Residues interacting with FXB are shown with carbons colored pink for residues from the C-terminal domain or cyan for residues from the N-terminal domain. Residues colored magenta are part of the C-terminal domain sequence but move in concert with the N-terminal domain.

database. When aligned, many of the sequences had an arginine at the positions found in either *E. coli* FhuD or *S. aureus* FhuD2, but there were also sequences lacking arginine at both of these positions. One of the sequences corresponded to PDB entry 3TNY, which is YfiY from *B. cereus* bound to the hydroxamate siderophore schizokinen. In this case, there are two arginine residues, one on each of the N- and C-terminal domains, and each makes hydrogen bonds to the schizokinen hydroxamates, effectively "sandwiching" the siderophore between the two domains. The alignment was sorted on the basis of the positions of the hydroxamate-binding arginine residues, indicating there are three related families of binding proteins

dx.doi.org/10.1021/bi401349d | *Biochemistry* 2014, 53, 2017−2031

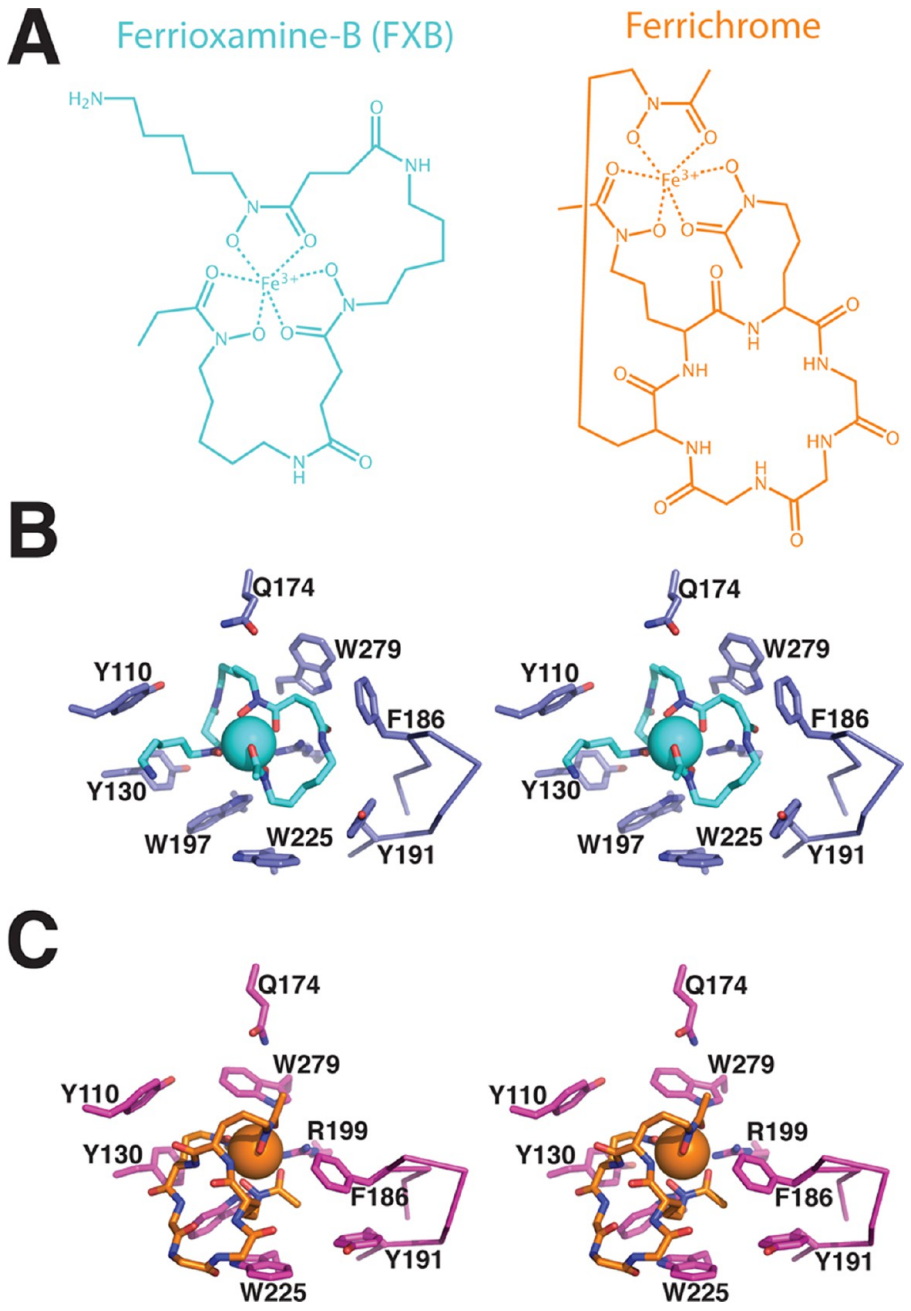

Figure 3. Comparison of ferrioxamine-B and ferrichrome binding by FhuD2. The ligand-binding site in the FhuD2−FXB complex is compared to that of FhuD2 bound to ferrichrome;[9] CA atoms of the entire structures were used for a least-squares superposition with an rmsd of 0.61 Å. (A) Chemical structures of the two iron-bound siderophores. (B) Current structure of FhuD2 bound to desferrioxamine-B. (C) Binding site of the FhuD2−ferrichrome complex,[9] with FhuD2 in exactly the same orientation as in panel B. The two siderophores are accommodated by local changes in the binding site, the most notable of which are the movement of the loop harboring F186 and the changes in the side chain conformations of Q174 and W279.

(Figure 4A; the full alignment and phylogenetic tree are provided as Supporting Information). In addition to the deposited crystal structure, the *B. cereus* YfiY protein has been analyzed biochemically and binds schizokinen with high affinity,[30] but the specificity of other members in the group has not been characterized.

The three different hydroxamate siderophore binding sites have evolved on an otherwise well-conserved type III binding protein platform. Type III binding proteins such as FhuD2 project two acidic groups from their surface, one on each domain. These acidic residues are required for the uptake of the siderophore by FhuD2,[1] and from structural studies of the related vitamin B_{12} (cobalamin) transporter, the position of the acidic residues is critical for productive interaction with the transporter's transmembrane domains.[31] In the case of FhuD2, the acidic residues are E97 on the N-terminal domain and E231 on the C-terminal domain (Figure 1). From the sequence alignment and a structural superposition of FhuD2, *E. coli* FhuD, and *B. cereus* YfiY (Figure 4B), it can be seen that despite the alternate configurations of the siderophore-binding residues, the positions of the acidic residues are very well conserved among the three family members.

dx.doi.org/10.1021/bi401349d | *Biochemistry* 2014, 53, 2017−2031

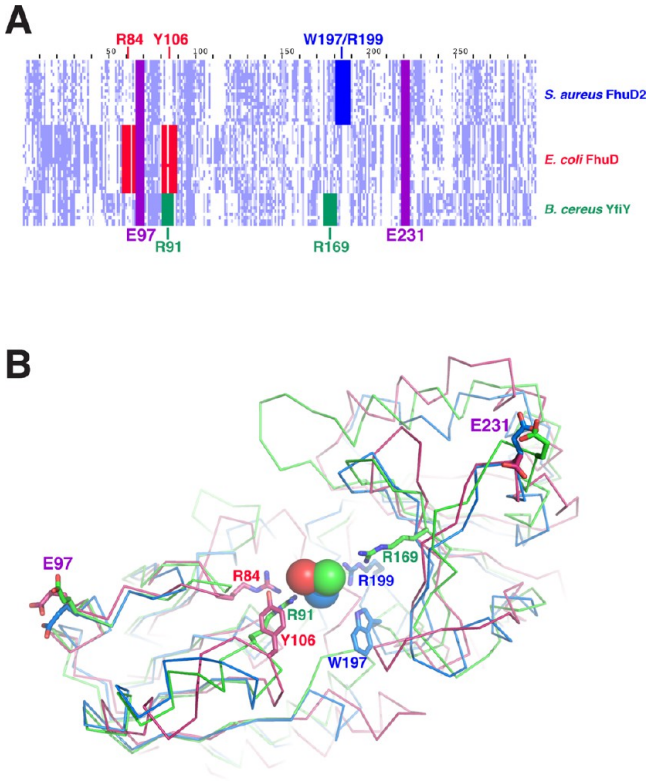

Figure 4. Sequence and structural alignment of three FhuD family members. (A) Graphical "bird's-eye" view of a sequence alignment of FhuD family members with the light purple shading indicating the degree of conservation at individual positions and the deep purple boxes showing the location of the almost perfectly conserved acidic residues required for transport (E97 and E231 in *S. aureus* FhuD2). The sequences were grouped into three families characterized by the presence of hydroxamate-binding residues on either the C-terminal domain (blue; W197 and R199 in *S. aureus* FhuD2), the N-terminal domain (red; R84 and Y106 in *E. coli* FhuD), or both (green; R91 and R169 in *B. cereus* YfiY). The full alignment and a corresponding phylogenetic tree are included as Figures S1 and S2, respectively, of the Supporting Information. (B) Three-dimensional structures of *S. aureus* FhuD2 (blue), *E. coli* FhuD (red; PDB entry 1K2V[39]), and *B. cereus* YfiY (green; PDB entry 3TNY[30]) were superimposed. The iron atoms are shown without the siderophore (for the sake of clarity) along with the key hydroxamate-binding residues. Conserved acidic residues, corresponding to *S. aureus* E97 and E231, are also indicated.

Rigid Body Domain Movements in Unliganded FhuD2. FhuD2 was crystallized in the absence of ligand to understand how siderophore binding affects its structure. Reductive methylation[11] of Se-Met-labeled FhuD2Δ43 changed the surface properties of FhuD2Δ43 so that it could be crystallized from solutions of methylpentanediol. These crystals diffracted to 2.2 Å resolution and were used to determine the structure of unliganded FhuD2 by MAD phasing (Table 3). Unmethylated FhuD2Δ24 readily formed crystals from high concentrations of ammonium sulfate, with the best crystals of unliganded FhuD2Δ24 yielding a 3.5 Å resolution data set (Table 2). These two crystal forms provided five molecules of unliganded FhuD2 in different conformations, indicating that there are a number of energetically similar states available to unliganded FhuD2.

For crystals of the unmodified and unliganded FhuD2Δ24, the C-terminal domains of three molecules interact to form a trimer in the asymmetric unit (Figure 5A). Each trimer interacts with three others by the formation of three FhuD2 dimers, in which loops (residues 184−189 and 246−253) from one molecule are inserted into the interdomain cleft of the second molecule (Figure 5B). Thus, crystal packing appears to have stabilized open conformations of FhuD2. The conformational differences among chains A−C in FhuD2Δ24 are due primarily to rigid body domain movements with a hinge region at residues 157−160 (Figure 6A). In the case of methylated FhuD2Δ43, the two molecules in the asymmetric unit are related by a smaller rigid body domain movement (Figure 6A). In addition to a good match for residues 50−150 in the N-terminal domain, the region including residues 276−287 in the C-terminal domain is relatively stationary. In fact, residues 276−287 of the C-terminal domain are in direct contact with the N-terminal domain and move in concert with it. Thus, with respect to the domain movements, the "N-terminal" domain consists of residues 47−158 and 276−287 while the C-terminal domain consists of residues 159−275 and 288−302.

In summary, the five molecules of unliganded FhuD2 occupy distinct conformations that are related by rigid body movements of the N- and C-terminal domains relative to each other. The observation of multiple unliganded conformations is consistent with small energetic differences between the conformations.

Ligand-Induced Conformational Change in FhuD2. Ligand-induced conformational changes in the class I and class II peripheral binding proteins of type I ABC import systems (such as the maltose transporter) are required for productive interactions with the membrane subunits and regulation of ATP hydrolysis.[32−34] For systems that incorporate a class III binding protein, such as the ferric hydroxamate uptake system or the vitamin B_{12} transporter, the role of ligand binding in the transport mechanism is still a matter of debate.[35,36] The availability of both the ligand-bound form of FhuD2 and several ligand-free conformations affords a unique opportunity to examine in detail the ligand-induced conformational change for a class III system.

The separation and relative positions of the conserved acidic residues E97 and E231 on the N- and C-terminal domains (Figure 4) can be used to characterize the changes in conformation in the FhuD2 crystal structures. The distance between the CA atoms of E97 and E231 of FhuD2 varies from 50.7, 52.4, and 52.7 Å for the A, B, and C chains of unliganded FhuD2Δ24, respectively, to 47.8 and 48.3 Å for the A and B chains of unliganded methylated FhuD2Δ43, respectively, and 44.9 Å for FXB-bound FhuD2Δ43 (Figure 7).

In addition to shortening the distance between E97 and E231, the FXB-induced conformational change has a different trajectory compared to that of the conformational changes observed in the unliganded forms. This can be seen in Figure 7A where the N-terminal domains have been superimposed and the CA positions for three of the unliganded conformations are plotted. The positions of E231 in the three unliganded conformations are close to colinear, while the position of E231 for the FXB-bound structure deviates from the trend. To develop this analysis further, the vectors between E97-CA and E231-CA were plotted for all five unliganded structures and the FXB-bound form (Figure 7B). The interatomic vectors between the E97 and E231 CA atoms in all five apo forms are nicely related by a line, from which the corresponding vector in FXB-bound FhuD2 deviates.

Solution Conformations of FhuD2. We had previously used SAXS to measure the solution conformation of the

dx.doi.org/10.1021/bi401349d | *Biochemistry* 2014, 53, 2017−2031

Table 3. Data Collection, Phasing, and Refinement Statistics for Methylated FhuD2Δ43

	remote	inflection	peak	falling edge
space group		$P2_12_12_1$		
unit cell		a = 66.0049, b = 75.2175, c = 100.9417		
wavelength (Å)	1.0000	0.9797	0.9795	0.9793
resolution[a]	60−2.20 (2.32−2.20)	60−2.20 (2.32−2.20)	60−2.20 (2.32−2.20)	60−2.20 (2.32−2.20)
no. of observations[a]	97675 (13069)	97858 (13112)	97932 (13140)	98043 (13167)
no. of unique observations[a]	26082 (3665)	26084 (3665)	26093 (3669)	26102 (3674)
completeness[a]	99.6 (98.1)	99.6 (98.2)	99.6 (98.3)	99.7 (98.4)
mean $I/\sigma I$[a]	14.0 (4.1)	15.3 (4.7)	16.1 (4.7)	15.9 (4.6)
R_{merge}[a]	0.056 (0.265)	0.057 (0.246)	0.057 (0.255)	0.057 (0.260)
phasing power (Iso/Ano)	−	1.24/2.78	1.01/2.31	0.90/2.28
figure of merit		0.651		
final model[b]	A, residues 47−302; B, residues 46−302; 4267 protein atoms; 217 solvent			
R/R_{free}	0.216/0.264			
rmsd				
bond lengths (Å)	0.0063			
bond angles (deg)	1.609			
dihedral angles (deg)	21.40			
improper angles (deg)	0.00			
B factor[c] (Å^2)				
all atoms	29.0			
main chain	26.4			
side chain	31.3			
solvent	30.6			

[a]Values in parentheses are for the highest-resolution shell. [b]Data collected at the peak wavelength were used for refinement. [c]Restrained isotropic B factor refinement.

FhuD2Δ24 construct[1] and found that both ferrichrome and FXB decreased the R_g from 20.6 Å for the apo form to 20.3 Å for ferrichrome and 20.5 Å for FXB. Rhodotorulic acid was also tested, and the R_g appeared to increase to 20.9 Å. The siderophore-dependent differences in R_g are intriguing, so we used the more compact FhuD2Δ43 construct to conduct a comprehensive analysis of its solution conformation.

Three or four SAXS measurements were made for apo FhuD2Δ43 and each of its complexes with ferrichrome, FXB, coprogen, and aerobactin. To facilitate comparison, the individual curves for the apo form and each of the four siderophores complexes were normalized to an $I(0)$ of 1, averaged, and plotted (Figure 8A,B). The curves all converge at 0.4 and 1.5 nm^{-1} (Figure 8A) and show their largest differences at 0.80 nm^{-1} (Figure 8B), indicating systematic differences in the shapes of the curves. To further illustrate the differences between the complexes, the apo data were subtracted from the data for each of the siderophore complexes to yield difference curves, which are plotted in Figure 8C. These curves show that the ferrichrome−FhuD2Δ43 complex exhibits the largest change from the apo form, while the aerobactin−FhuD2Δ43 complex shows the smallest change. Siderophore binding led to a decrease in the radius of gyration (R_g) compared to that of the unliganded protein, and consistent with the plots in Figure 8, each complex appeared to have a unique R_g (Table 4). The differences in the R_g values were paralleled by decreases in the V_c parameter, which is defined as the ratio of the zero-angle [$I(0)$] scattering intensity to the total scattered intensity and is dependent on the conformation of the protein.[25] Additionally, the volume of the scattering particles was calculated from the SAXS data[24] and shows a decrease upon going from the unliganded form, with the largest volume, to the ferrichrome-bound form, with the smallest volume (Table 4). The molecular weight, calculated either from the FhuD2 SAXS data alone,[25] or by comparison with a cytochrome c standard, shows that FhuD2 behaved as a monomer in all cases. In summary, the current SAXS study with the FhuD2Δ43 construct supports our previous observations that binding of different hydroxamate siderophores to FhuD2 leads to a compaction of the protein, the extent of which depends on the identity of the siderophore.

These are the first SAXS measurements for a class III solute binding protein for which crystal structures have also been determined. To gain additional insight into the structure and dynamics of FhuD2, the crystal structures were compared to the averaged solution scattering data. The crystal structures of FXB-bound FhuD2 and the complex with ferrichrome[3] are very similar, with an rmsd for all CA atoms of 0.61 Å and calculated R_g values of 18.8 and 19.1 [for the nonhydrated structures (Table 5)]. The slightly larger R_g for the crystal structure of the FhuD2−ferrichrome complex is surprising given that SAXS data indicate the FhuD2−ferrichrome complex is more compact than the FhuD2−FXB complex in solution. In addition, the crystal structures of FXB- and ferrichrome-bound FhuD2 demonstrate the best agreement with the solution SAXS data from the FhuD2−aerobactin complex (Table 5). Surprisingly, the two ligand-bound crystal structures appear to be slightly less compact than the ligand-bound forms

dx.doi.org/10.1021/bi401349d | Biochemistry 2014, 53, 2017−2031

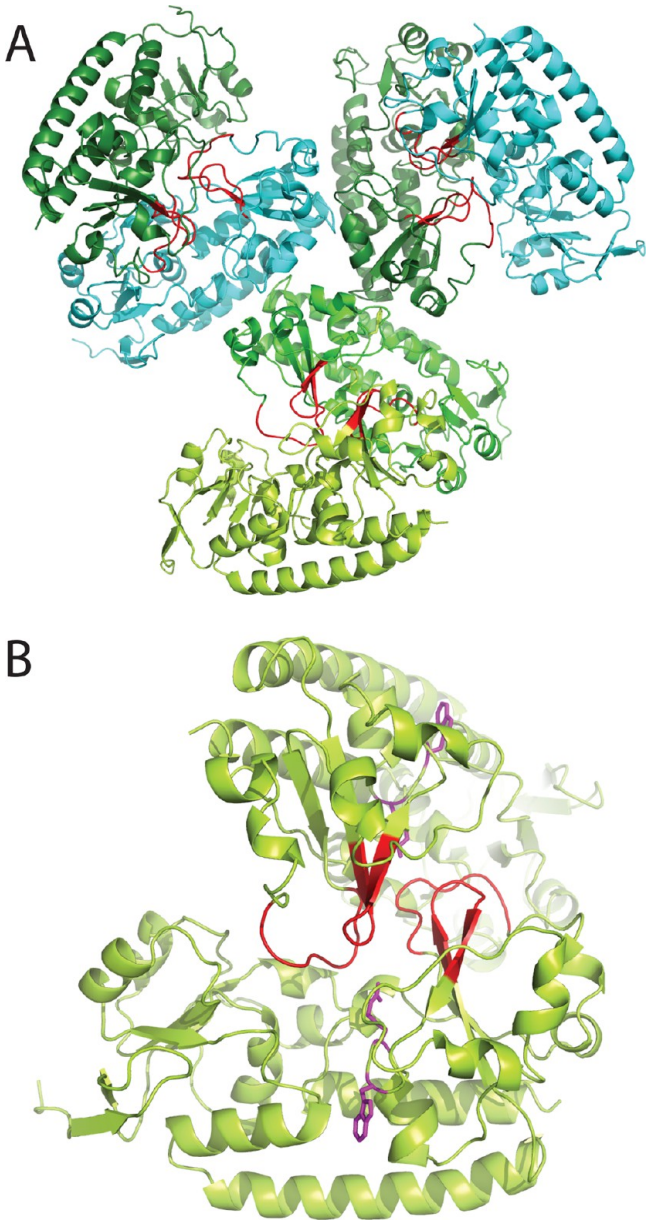

Figure 5. Crystal packing in unliganded FhuD2Δ24. (A) Trimer of FhuD2Δ24 that is present in the asymmetric unit of the crystal, along with three monomers from crystallographically related trimers. The A chain (bottom, light green) forms a symmetric dimer with the A chain from a neighboring trimer, while the B chain (cyan) and C chain (dark green) form asymmetric dimers with the C and B chains from neighboring trimers. Residues 184−191 and 246−253 are colored red. These loops are positioned in the interdomain cleft of symmetry-related molecules. (B) Focus on the symmetric dimer formed by the A chain. In addition to the loop residues colored red, as in panel B, the two residues that are critical for hydroxamate binding, W197 and R199, are colored magenta to illustrate the location of the siderophore binding site.

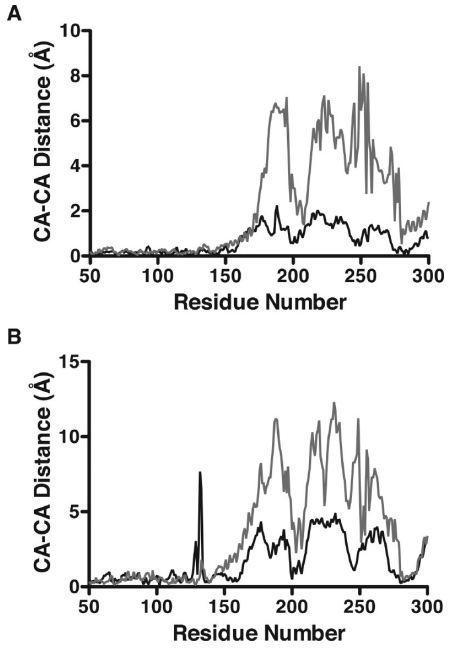

Figure 6. Rigid body domain movements in unliganded and FXB-bound FhuD2. Residues 50−150 were used to superimpose the N-terminal domains of FhuD2 molecules onto one another; distances between corresponding CA positions through the whole sequence are plotted. (A) Conformational differences between unliganded FhuD2 molecules show they are related by a rigid body domain movement. The black plot maps the CA distances between the two molecules in the asymmetric unit of methylated and unliganded FhuD2Δ43; the gray plot maps the CA distances between the A and C chains found in crystals of unliganded FhuD2Δ24. (B) Conformational differences between liganded and unliganded FhuD2 molecules indicate a rigid body domain movement upon ligand binding. The black plot maps the CA distances between FXB-bound FhuD2 and the A chain of methylated, unliganded FhuD2Δ43; the gray plot maps CA distances between FXB-bound FhuD2 and the C chain of unliganded FhuD2Δ24.

in solution, and the ferrichrome-bound structure in the crystal adopts the same conformation as FXB-bound FhuD2 or perhaps a conformation slightly less compact than that of FXB-bound FhuD2, which is the opposite of what is observed in solution. It appears that crystal packing has selected for a single conformation of siderophore-bound FhuD2, whereas in solution, the protein adopts slightly different conformations depending on the identity of the siderophore. In this regard, it is noteworthy that the various siderophores display different abilities to support growth on iron-limited media,[1] an effect that may have its origins in the siderophore-dependent structural and/or dynamic differences in FhuD2.

For unliganded FhuD2, the different conformations observed in the crystals are all more extended than the conformation of unliganded FhuD2 in solution. Crystal packing can select for species that are present in minor amounts in solution, but one expects that the conformations observed in the crystal will represent relatively low-energy forms that are sampled in solution. On the basis of the solution SAXS results, unliganded FhuD2 exists predominantly in a relatively compact state, close to what is observed for the ligand-bound forms, and the extended forms observed in the crystals are likely present in only very small quantities in solution. On the basis of a comparison with the vitamin B_{12} transport system in which an extended form of the binding protein is present when bound to the membrane subunits,[31,37,38] we suggest that the extended conformations of unliganded FhuD2 captured by crystallization may play an important role in the transport mechanism.

DISCUSSION

Type II ABC import systems and associated class III binding proteins play critical roles in the uptake of iron by bacteria, facilitating growth under iron-limited conditions. Along these

dx.doi.org/10.1021/bi401349d | Biochemistry 2014, 53, 2017−2031

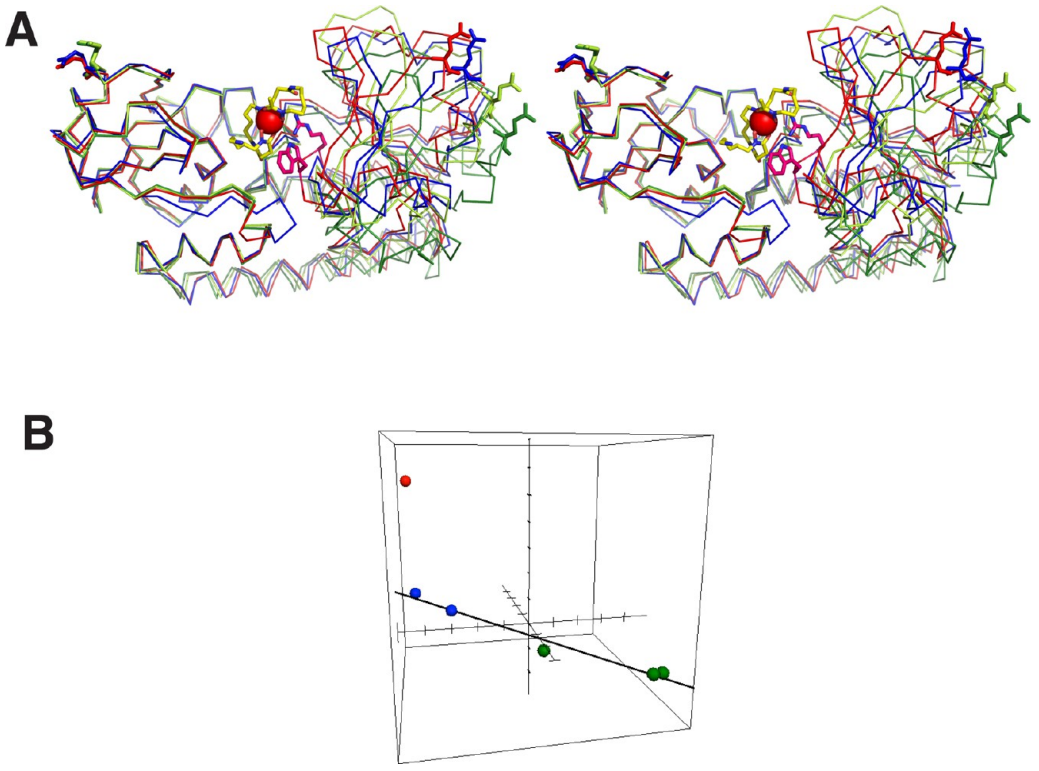

Figure 7. Conformational changes in crystals of FhuD2. Residues 50−150 were used to superimpose the N-terminal domains of FhuD2 molecules. (A) The CA traces of the A and C chains of unliganded FhuD2Δ24 are colored light and dark green, respectively; the A chain of unliganded, methylated FhuD2Δ43 is colored blue, and FhuD2Δ43-FXB is colored red. (B) Vectors between E97 and E231 CA positions were calculated and their end points plotted. The three green points represent the A, B, and C chains of unliganded FhuD2Δ24; the blue points represent the A and B chains of unliganded, methylated FhuD2Δ43, and the red point represents FXB-bound FhuD2Δ43. Principal component analysis was used to determine a line through the CA positions of the five apo forms.

lines, the *S. aureus* Fhu system has garnered additional interest since Novartis Vaccines recently identified FhuD2 as a virulence factor and leading vaccine candidate.[3]

One of the fascinating aspects of the Fhu systems is their ability to acquire a number of different hydroxamate siderophores. There are now two structures of ligand-bound FhuD2: one with bound ferrichrome[9] and the current structure with bound FXB. From these structures, we know that R199 and W197 play a key role in the bonding of hydrogen to the common hydroxamate moieties of the two siderophores, while a ring of mostly aromatic residues accommodates the aliphatic, and structurally divergent, portions of the siderophores. This mode of binding is similar to that seen for *E. coli* FhuD, which was originally determined with gallichrome[10] (gallium-substituted ferrichrome) and subsequently with a variety of other hydroxamate siderophores, including FXB.[39] In all cases, the same two residues, R84 and Y106, bind to the common hydroxamate functions of the siderophores, while aromatic residues accommodate other parts of the siderophores. Therefore, both proteins use similar chemistry and a common binding site to accommodate a variety of different hydroxamate siderophores. The main difference between the two proteins is that the binding site is on the C-terminal domain of *S. aureus* FhuD2 while it is on the N-terminal domain of *E. coli* FhuD. A group of closely related proteins, whose structure is represented by that of *B. cereus* YfiY (PDB entry 3TNY[30]), uses a different mode of binding, in which the hydroxamates are bound by two arginine residues, one on the N-terminal domain and one on the C-terminal domain. It is not yet clear whether proteins in this group are able to bind siderophores such as ferrichrome and FXB, in common with *S. aureus* FhuD2 and *E. coli* FhuD.

Solution X-ray scattering measurements indicate that binding of particular siderophores to FhuD2 leads to distinct conformations. With respect to transport function, it is also clear that different siderophores are transported with varying efficiencies. These differences in transport efficiencies cannot normally be detected in the wild-type system, but mutation of key acidic residues involved in interaction with the membrane subunits, namely, E97 and/or E231, yields observable differences in growth depending on which siderophore is supplied in the medium.[1] For example, *S. aureus* expressing FhuD2-(E231A) or FhuD2(E231Q) exhibits wild-type growth on aerobactin, coprogen, and ferrichrome but is severely compromised for growth on FXB and rhodotorulic acid. More generally, FhuD2 with mutations in E97 and/or E231 transports ferrichrome efficiently, but transport of FXB tends to be severely compromised. These differences in transport efficiency may have their origin in siderophore-specific effects on the structure and dynamics of FhuD2, or they could be due to differences in the interaction of the siderophores with the membrane subunits.

For ABC import systems, the crystal structures and solution conformations of solute binding proteins can provide insight into their roles in the transport cycle. For class I systems, the binding proteins have been characterized by a "venus fly trap" model[5] because in the absence of ligand the proteins exist in an open conformation that is clearly distinct from the ligand-bound closed conformation. In the case of the maltose transporter, the closed ligand-bound form of maltose binding

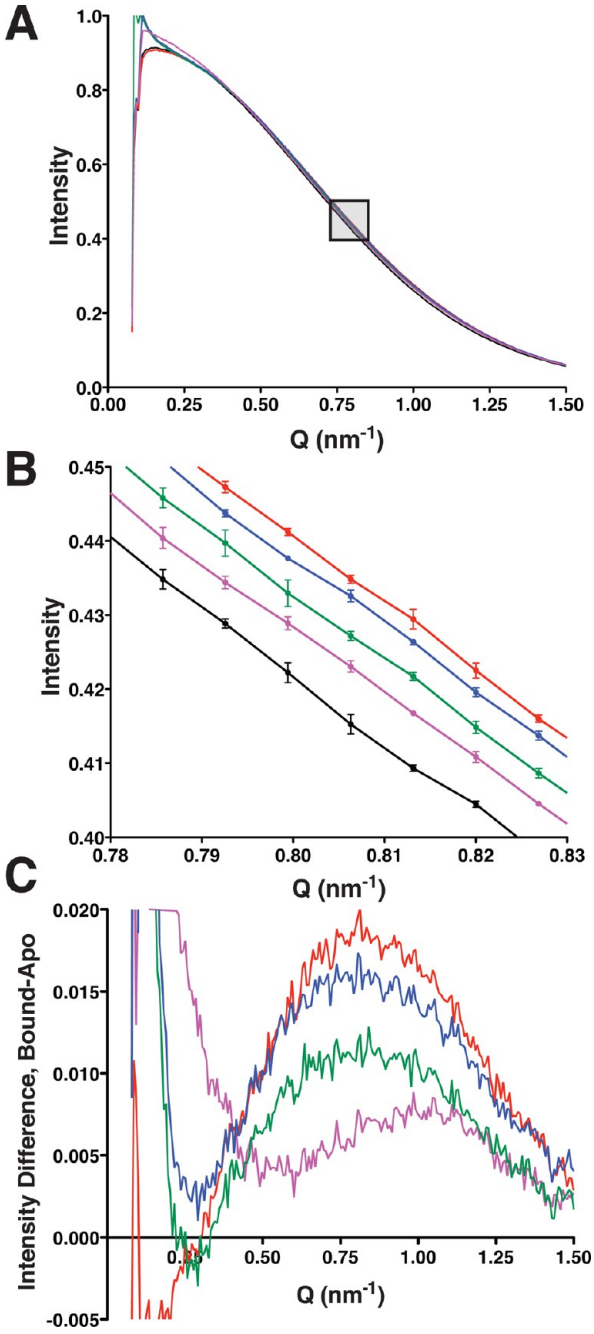

Figure 8. Siderophore-induced changes in the FhuD2 solution conformation. Small-angle X-ray scattering (SAXS) was used to measure the changes in the solution structure of FhuD2 in response to siderophore binding. The protein concentration was 5.4 mg/mL (180 μM), and the siderophore concentrations were 300 μM. (A) The averaged scattering curves (from three measurements each) for apo FhuD2 (black) and for FhuD2 with aerobactin (magenta), coprogen (green), ferrioxamine B (blue), or ferrichrome (red) were normalized to a forward scattering value of 1 and superimposed. The curves converge at Q values of approximately 0.4 and 1.5 nm^{-1}, while they diverge in the mid-angle region. The shaded area in the scattering region of 0.8 nm^{-1} is magnified in panel B to show the differences in the average curves along with the associated standard deviations for the SAXS measurements. (C) To highlight the siderophore-induced conformational changes, difference curves were calculated by subtracting the scattering by unliganded FhuD2 from the scattering curve recorded in the presence of aerobactin (magenta), coprogen (green), ferrioxamine B (blue), or ferrichrome (red).

protein (MBP) binds to, and presumably stabilizes, an intermediate-occluded conformation of the membrane subunits, thereby promoting a conformational change in the system.[32,40,41] This leads to adoption of the transition state for ATP hydrolysis, in which the open conformation of MBP is tightly bound to the membrane subunits with the ABC subunits poised to hydrolyze ATP.[42] The Fhu system is a class II ABC import system and FhuD2 a type III solute binding protein, and there are differences in the way these systems work,[35] although one expects that both the ligand-bound and unliganded proteins will have critical roles in transport and the regulation of ATPase activity, just as they do for the class I transport systems.

For FhuD2 in complex with its siderophore ligands, these SAXS studies with the FhuD2Δ43 construct, as well as those conducted previously with the longer FhuD2Δ24 construct,[1] indicate that FhuD2 adopts slightly different solution conformations depending on which siderophore is bound. This is perhaps not so surprising because one might expect that binding of the various siderophore structures would stabilize slightly different domain orientations in FhuD2. In this respect, it is interesting that *E. coli* FhuD has been crystallized with several different siderophores, and in all cases, the crystallized conformations are identical.[10,39] For the FXB-bound FhuD2 crystals in this work, all four NCS-related molecules were in exactly the same conformation; furthermore, the structure of the ferrichrome−FhuD2 complex is almost identical in conformation to the structure of the FXB−FhuD2 complex even though it was crystallized in a completely different space group.[9] In addition, FhuD2 crystallized with ferrichrome or FXB shows the greatest structural resemblance to the solution conformation of FhuD2 with aerobactin. Thus, crystallization of ligand-bound FhuD2 appears to select for a particular common conformation that is slightly different from what is observed in solution. It would be interesting to know whether this is true for other type III binding proteins. In any case, our SAXS studies indicate that the ligand-induced change in conformation, which is almost insignificant for binding of aerobactin (this study) or rhodoturulic acid,[1] cannot explain how binding of a ligand to FhuD2 regulates the activity of the transporter. Instead, ligand binding likely induces a change in the dynamics of the protein, stabilizing a particular conformation that in turn can affect the structure and/or dynamics of the FhuBG membrane complex.

What can the current studies with unliganded FhuD2 tell us about the function of the type III binding proteins in class II ABC import systems? SAXS measurements indicate that crystallization of unliganded FhuD2 has captured extended conformations that are only minor species in solution; however, we believe these conformations play an important role in the transport cycle. In the case of the vitamin B_{12} transporter, the most extended conformation of the binding protein, BtuF, occurs when it is bound to the membrane subunits. Although there are no solution data available for BtuF, the protein was crystallized with two molecules in the asymmetric unit, providing two structures of the unliganded protein, with R_g values of 18.7 and 19.2 Å, and two structures of the ligand-bound protein, each with an R_g of 19.0 Å. Thus, from the crystallographic studies, ligand binding has a relatively small and inconsistent effect on the conformation of BtuF. In contrast, when bound to BtuCD, BtuF has an R_g of 19.8 Å in all of the available structures. This increase in R_g can be explained by the insertion of residues 174−186 from the BtuC membrane

dx.doi.org/10.1021/bi401349d | *Biochemistry* 2014, 53, 2017−2031

Table 4. Solution Structure Parameters of FhuD2

				M_R (kDa)	
sample[a]	R_g (Å)	V_c[b] (Å^2)	Porod volume[c] (Å^3)	Q_R[d]	cytochrome c[e]
unliganded	20.0 ± 0.15	260 ± 2.8	39900 ± 220	27.4 ± 0.4	26.5 ± 0.1
aerobactin	19.9 ± 0.04	250 ± 1.4	39500 ± 190	25.6 ± 0.2	29.0 ± 0.1
coprogen	19.8 ± 0.19	252 ± 3.0	39300 ± 290	25.9 ± 0.4	26.6 ± 0.2
FXB	19.7 ± 0.11	248 ± 1.8	39000 ± 373	25.3 ± 0.3	27.0 ± 0.1
ferrichrome	19.5 ± 0.05	246 ± 2.4	38600 ± 204	25.4 ± 0.5	28.8 ± 0.04

[a]All results are means ± the standard deviation for three measurements at a FhuD2 concentration of 5.4 mg/mL. [b]The ratio of zero-angle scattering to total scattering for a single SAXS curve.[25] [c]Determined using Primus[23] following the method of Rambo and Tainer.[24] [d]Calculated from the empirically determined relationship between Q_R (V_c^2/R_g) and molecular weight.[25] [e]Determined by comparison with a cytochrome c standard.

Table 5. Comparison between Solution and Crystal Structures

			agreement with solution SAXS data[a] (χ)				
FhuD2 structure	chain	R_g[a] (Å)	apo	aerobactin	coprogen	FXB	ferrichrome
FXB-bound	A	18.8	4.2	0.94	1.2	1.4	2.4
ferrichrome[9]	A	19.1	4.8	1.3	1.7	1.9	3.2
unliganded	A	19.7	8.4	3.1	3.5	4.0	6.0
	B	19.9	9.7	3.6	4.0	4.6	6.8
	C	20.0	10.0	4.6	4.1	4.8	7.1
unliganded (methylated)	A	19.4	7.5	3.0	3.2	3.6	5.5
	B	19.5	8.0	3.6	3.4	3.9	6.0

[a]The R_g (nonhydrated structures) and χ values were calculated using the FoXs server.[26,45]

subunits into the empty binding site of BtuF, which will stabilize the more extended conformation of BtuF. Similarly, in the case of FhuD2, the highly extended conformations occur when crystal contacts result in the insertion of loop regions into the ligand binding site (Figure 5); thus, crystal packing may mimic what happens to the binding protein during transport. The functional significance for transport is that insertion of loops from the membrane subunits into the ligand binding site of the peripheral binding protein ensures that the ligand has migrated from its high-affinity site in the binding protein to a lower-affinity site in the integral membrane subunits. In the case of the maltose transporter, there is evidence that this mechanism plays a key role in coupling ATP hydrolysis to substrate translocation:[43,44] insertion of a loop from MalG into the binding site of MBP ensures that maltose has moved into the binding site of the integral membrane subunits (MalFG) before ATP is hydrolyzed. A related mechanism may be operative in the class II systems. In particular, the insertion of residues from the membrane subunit into BtuF (or FhuD2) may stabilize the extended conformations that, in turn, affect the structure and dynamics of the membrane integral and ABC subunits.

■ ASSOCIATED CONTENT

Supporting Information

Full sequence alignment for *E. coli* FhuD and *S. aureus* FhuD2 and related proteins, corresponding to the graphic in Figure 4A (Figure S1), and the corresponding phylogenetic tree (Figure S2). This material is available free of charge via the Internet at http://pubs.acs.org.

■ AUTHOR INFORMATION

Corresponding Author

*Department of Biochemistry, The University of Western Ontario, 1151 Richmond St., London, Ontario, Canada N6A 5C1. E-mail: bshilton@uwo.ca. Telephone: (519) 661-4124. Fax: (519) 661-3175.

Funding

This work was supported by an NSERC Discovery grant to B.H.S. and a Canadian Institutes of Health Research grant to D.E.H.

Notes

The authors declare no competing financial interest.

■ ACKNOWLEDGMENTS

Thanks to Greg Gloor for helpful discussion. Use of the Advanced Photon Source is supported by the U.S. Department of Energy, Basic Energy Sciences, Office of Science, under Contract W-31-109-ENG-38, and BioCAT is supported by National Institutes of Health Grant RR-08630.

■ REFERENCES

(1) Sebulsky, M. T., Shilton, B. H., Speziali, C. D., and Heinrichs, D. E. (2003) The role of FhuD2 in iron(III)-hydroxamate transport in *Staphylococcus aureus*. Demonstration that FhuD2 binds iron(III)-hydroxamates but with minimal conformational change and implication of mutations on transport. *J. Biol. Chem. 278*, 49890−49900.

(2) Sebulsky, M. T., Speziali, C. D., Shilton, B. H., Edgell, D. R., and Heinrichs, D. E. (2004) FhuD1, a ferric hydroxamate-binding lipoprotein in *Staphylococcus aureus*: A case of gene duplication and lateral transfer. *J. Biol. Chem. 279*, 53152−53159.

(3) Mishra, R. P. N., Mariotti, P., Fiaschi, L., Nosari, S., Maccari, S., Liberatori, S., Fontana, M. R., Pezzicoli, A., De Falco, M. G., Falugi, F., Altindis, E., Serruto, D., Grandi, G., and Bagnoli, F. (2012) *Staphylococcus aureus* FhuD2 is involved in the early phase of staphylococcal dissemination and generates protective immunity in mice. *J. Infect. Dis. 206*, 1041−1049.

(4) Braun, V., Pramanik, A., Gwinner, T., Köberle, M., and Bohn, E. (2009) Sideromycins: Tools and antibiotics. *BioMetals 22*, 3−13.

(5) Quiocho, F. A., and Ledvina, P. S. (1996) Atomic structure and specificity of bacterial periplasmic receptors for active transport and chemotaxis: Variation of common themes. *Mol. Microbiol. 20*, 17−25.

(6) Bishop, L., Agbayani, R., Ambudkar, S. V., Maloney, P. C., and Ames, G. F. (1989) Reconstitution of a bacterial periplasmic permease

in proteoliposomes and demonstration of ATP hydrolysis concomitant with transport. *Proc. Natl. Acad. Sci. U.S.A. 86*, 6953−6957.
(7) Davidson, A., Shuman, H., and Nikaido, H. (1992) Mechanism of maltose transport in *Escherichia coli*: Transmembrane signaling by periplasmic binding proteins. *Proc. Natl. Acad. Sci. U.S.A. 89*, 2360−2364.
(8) Berntsson, R. P.-A., Smits, S. H. J., Schmitt, L., Slotboom, D.-J., and Poolman, B. (2010) A structural classification of substrate-binding proteins. *FEBS Lett. 584*, 2606−2617.
(9) Mariotti, P., Malito, E., Biancucci, M., Surdo, L. P., Mishra, R. P. N., Nardi-Dei, V., Savino, S., Nissum, M., Spraggon, G., Grandi, G., Bagnoli, F., and Bottomley, M. J. (2013) Structural and functional characterization of the *Staphylococcus aureus* virulence factor and vaccine candidate FhuD2. *Biochem. J. 449*, 683−693.
(10) Clarke, T. E., Ku, S. Y., Dougan, D. R., Vogel, H. J., and Tari, L. W. (2000) The structure of the ferric siderophore binding protein FhuD complexed with gallichrome. *Nat. Struct. Biol. 7*, 287−291.
(11) Rayment, I. (1997) Reductive alkylation of lysine residues to alter crystallization properties of proteins. *Methods Enzymol. 276*, 171−179.
(12) Majeed, S., Ofek, G., Belachew, A., Huang, C., Zhou, T., and Kwong, P. (2003) Enhancing Protein Crystallization through Precipitant Synergy. *Structure 11*, 1061−1070.
(13) Derewenda, Z. S. (2004) Rational protein crystallization by mutational surface engineering. *Structure 12*, 529−535.
(14) Weeks, C. M., Blessing, R. H., Miller, R., Mungee, R., Potter, S. A., Rappleye, J., Smith, G. D., Xu, H., and Furey, W. (2002) Towards automated protein structure determination: BnP, the SnB-PHASES interface. *Z. Kristallogr. 217*, 686−693.
(15) Langer, G., Cohen, S. X., Lamzin, V. S., and Perrakis, A. (2008) Automated macromolecular model building for X-ray crystallography using ARP/wARP version 7. *Nat. Protoc. 3*, 1171−1179.
(16) Brunger, A. T., Adams, P. D., Clore, G. M., DeLano, W. L., Gros, P., Grosse-Kunstleve, R. W., Jiang, J. S., Kuszewski, J., Nilges, M., Pannu, N. S., Read, R. J., Rice, L. M., Simonson, T., and Warren, G. L. (1998) Crystallography & NMR system: A new software suite for macromolecular structure determination. *Acta Crystallogr. D54*, 905−921.
(17) Hayward, S., and Berendsen, H. J. (1998) Systematic analysis of domain motions in proteins from conformational change: New results on citrate synthase and T4 lysozyme. *Proteins 30*, 144−154.
(18) Read, R. J., and Sussman, J. L., Eds. (2007) Likelihood-based Molecular Replacement in Phaser. In *Evolving Methods for Macromolecular Crystallography*, pp 91−100, Springer, Berlin.
(19) Adams, P. D., Afonine, P. V., Bunkóczi, G., Chen, V. B., Davis, I. W., Echols, N., Headd, J. J., Hung, L.-W., Kapral, G. J., Grosse-Kunstleve, R. W., McCoy, A. J., Moriarty, N. W., Oeffner, R., Read, R. J., Richardson, D. C., Richardson, J. S., Terwilliger, T. C., and Zwart, P. H. (2010) PHENIX: A comprehensive Python-based system for macromolecular structure solution. *Acta Crystallogr. D66*, 213−221.
(20) Raymond, K., Müller, G., and Matzanke, B. (1984) Complexation of Iron by Siderophores: A Review of Their Solution and Structural Chemistry and Biological Function. In *Topics in Current Chemistry*, pp 49−102, Springer, Berlin.
(21) Dhungana, S., White, P. S., and Crumbliss, A. L. (2001) Crystal structure of ferrioxamine B: A comparative analysis and implications for molecular recognition. *JBIC, J. Biol. Inorg. Chem. 6*, 810−818.
(22) Semenyuk, A., and Svergun, D. (1991) GNOM: A program package for small-angle scattering data processing. *J. Appl. Crystallogr. 24*, 537−540.
(23) Konarev, P. V., Volkov, V. V., Sokolova, A. V., Koch, M. H., and Svergun, D. I. (2003) PRIMUS: A Windows PC-based system for small-angle scattering data analysis. *J. Appl. Crystallogr. 36*, 1277−1282.
(24) Rambo, R. P., and Tainer, J. A. (2011) Characterizing flexible and intrinsically unstructured biological macromolecules by SAS using the Porod-Debye law. *Biopolymers 95*, 559−571.
(25) Rambo, R. P., and Tainer, J. A. (2013) Accurate assessment of mass, models and resolution by small-angle scattering. *Nature 496*, 477−481.
(26) Schneidman-Duhovny, D., Hammel, M., and Sali, A. (2010) FoXS: A web server for rapid computation and fitting of SAXS profiles. *Nucleic Acids Res. 38*, W540−W544.
(27) Waterhouse, A. M., Procter, J. B., Martin, D. M. A., Clamp, M., and Barton, G. J. (2009) Jalview Version 2: A multiple sequence alignment editor and analysis workbench. *Bioinformatics 25*, 1189−1191.
(28) Poirot, O., Suhre, K., Abergel, C., O'Toole, E., and Notredame, C. (2004) 3DCoffee@igs: A web server for combining sequences and structures into a multiple sequence alignment. *Nucleic Acids Res. 32*, W37−W40.
(29) Dereeper, A., Guignon, V., Blanc, G., Audic, S., Buffet, S., Chevenet, F., Dufayard, J.-F., Guindon, S., Lefort, V., Lescot, M., Claverie, J.-M., and Gascuel, O. (2008) Phylogeny.fr: robust phylogenetic analysis for the non-specialist. *Nucleic Acids Res. 36*, W465−W469.
(30) Zawadzka, A. M., Abergel, R. J., Nichiporuk, R., Andersen, U. N., and Raymond, K. N. (2009) Siderophore-mediated iron acquisition systems in *Bacillus cereus*: Identification of receptors for anthrax virulence-associated petrobactin. *Biochemistry 48*, 3645−3657.
(31) Hvorup, R. N., Goetz, B. A., Niederer, M., Hollenstein, K., Perozo, E., and Locher, K. P. (2007) Asymmetry in the structure of the ABC transporter-binding protein complex BtuCD-BtuF. *Science 317*, 1387−1390.
(32) Shilton, B. H. (2008) The dynamics of the MBP-MalFGK(2) interaction: A prototype for binding protein dependent ABC-transporter systems. *Biochim. Biophys. Acta 1778*, 1772−1780.
(33) Oldham, M. L., Davidson, A. L., and Chen, J. (2008) Structural insights into ABC transporter mechanism. *Curr. Opin. Struct. Biol. 18*, 726−733.
(34) Schneider, E., Eckey, V., Weidlich, D., Wiesemann, N., Vahedi-Faridi, A., Thaben, P., and Saenger, W. (2012) Receptor-transporter interactions of canonical ATP-binding cassette import systems in prokaryotes. *Eur. J. Cell Biol. 91*, 311−317.
(35) Locher, K. P. (2009) Structure and mechanism of ATP-binding cassette transporters. *Philos. Trans. R. Soc., B 364*, 239−245.
(36) Lewinson, O., Lee, A. T., Locher, K. P., and Rees, D. C. (2010) A distinct mechanism for the ABC transporter BtuCD-BtuF revealed by the dynamics of complex formation. *Nat. Struct. Mol. Biol. 17*, 332−338.
(37) Korkhov, V. M., Mireku, S. A., Hvorup, R. N., and Locher, K. P. (2012) Asymmetric states of vitamin B_{12} transporter BtuCD are not discriminated by its cognate substrate binding protein BtuF. *FEBS Lett. 586*, 972−976.
(38) Korkhov, V. M., Mireku, S. A., and Locher, K. P. (2012) Structure of AMP-PNP-bound vitamin B_{12} transporter BtuCD-F. *Nature 490*, 367−372.
(39) Clarke, T. E., Braun, V., Winkelmann, G., Tari, L. W., and Vogel, H. J. (2002) X-ray crystallographic structures of the *Escherichia coli* periplasmic protein FhuD bound to hydroxamate-type siderophores and the antibiotic albomycin. *J. Biol. Chem. 277*, 13966−13972.
(40) Orelle, C., Ayvaz, T., Everly, R. M., Klug, C. S., and Davidson, A. L. (2008) Both maltose-binding protein and ATP are required for nucleotide-binding domain closure in the intact maltose ABC transporter. *Proc. Natl. Acad. Sci. U.S.A. 105*, 12837−12842.
(41) Oldham, M. L., and Chen, J. (2011) Crystal structure of the maltose transporter in a pretranslocation intermediate state. *Science 332*, 1202−1205.
(42) Oldham, M. L., Khare, D., Quiocho, F. A., Davidson, A. L., and Chen, J. (2007) Crystal structure of a catalytic intermediate of the maltose transporter. *Nature 450*, 515−521.
(43) Gould, A. D., and Shilton, B. H. (2010) Studies of the maltose transport system reveal a mechanism for coupling ATP hydrolysis to substrate translocation without direct recognition of substrate. *J. Biol. Chem. 285*, 11290−11296.
(44) Cui, J., Qasim, S., and Davidson, A. L. (2010) Uncoupling substrate transport from ATP hydrolysis in the *Escherichia coli* maltose transporter. *J. Biol. Chem. 285*, 39986−39993.

(45) Schneidman-Duhovny, D., Hammel, M., Tainer, J. A., and Sali, A. (2013) Accurate SAXS Profile Computation and its Assessment by Contrast Variation Experiments. *Biophys. J. 105*, 962−974.